1276 *Chem. Mater.* **2010,** *22,* 1276–1278
DOI:10.1021/cm903303v

CHEMISTRY OF MATERIALS
Communication

Facile Method To Synthesize Mesoporous Multimetal Oxides ($ATiO_3$, A = Sr, Ba) with Large Specific Surface Areas and Crystalline Pore walls

Xiaoxing Fan,[†,§] Ying Wang,[†,§] Xinyi Chen,[†] Ling Gao,[§] Wenjun Luo,[†] Yupeng Yuan,[†] Zhaosheng Li,[†,‡] Tao Yu,[†] Jianhua Zhu,[§] and Zhigang Zou*[,†]

[†]*Ecomaterials and Renewable Energy Research Center, Department of Physics and National Laboratory of Solid State Microstructures, Nanjing University, Nanjing, China,* [‡]*Department of Materials Science and Engineering, Nanjing University, Nanjing, China, and* [§]*School of Chemistry and Chemical Engineering, Nanjing University, 22 HanKou Road, Nanjing, China*

Received October 28, 2009
Revised Manuscript Received December 23, 2009

Mesoporous metal oxides have attracted growing interest because their dielectric, photoelectric, or photocatalytic properties can be improved due to their mesostructures.[1−3] However, very little progress has been made in relation to the syntheses of mesoporous multimetal oxides.

The evaporation-induced self-assembly (EISA) approach is one of the most efficient techniques for synthesizing mesoporous single-metal oxides,[4−6] but it has not been extended to mesoporous multimetal oxides due to two problems. One is the phase separation caused by heterogeneity in the solubility of the nonvolatile components during the solvent evaporation process.[7] To obtain mesoporous multimetal oxides with pure phases, the cations of the starting sol must be homogeneously mixed on the molecular scale. If not, the as-prepared samples usually contain secondary phases.[8] Chelating agents such as acetylacetone, ethylene glycol, and triethanolamine are often used to achieve homogeneous mixing of the starting sol. However, these chelating agents usually lead to the production of poor nanobuilding blocks for mesostructures.[9,10] The second problem is the thermal stability of the mesostructures of multimetal oxides. Organic surfactants used in the EISA method usually decompose below the crystallization temperatures of the multimetal oxides. The mesostructures always collapse as a result of both the pore-wall crystallization and the lack of support at high calcination temperatures, while low calcination temperatures result in the formation of amorphous phases or impurities. There are a few reports dealing with the syntheses of mesoporous multimetal oxides.[11−15] In particular in 2004, Grosso et al. synthesized mesoporous multimetal oxide films including $SrTiO_3$ films, by using a special organic template (KLE3739), which allowed fast mesophase formation with all metal species, to be solubilized into the flexible and condensable networks.[11] However, reports concerning the syntheses of mesoporous multimetal oxides all concentrated on organic pore-makers and not on inorganic pore-makers.

Here, we propose a new strategy to synthesize mesoporous multimetal oxides such as $SrTiO_3$ and $BaTiO_3$ by using in situ inorganic pore-makers based on the EISA approach. When synthesizing mesoporous $SrTiO_3$, for example, a Sr/Ti ratio of 1:1 is traditionally used in a sol−gel synthesis. However, in our strategy, either a 1.5:1 or a 2:1 ratio will be adopted, where the Sr metal precursor will be in excess. Following solvent evaporation and calcination, the excess Sr precursor partly reacts to form multimetal oxides and partly turns into nanoscale grains ($SrCO_3$) dispersed in the sample. Then, the mesostructure is obtained by the removal of carbonate with acid. This strategy has two advantages. First, the adopted inorganic pore-makers are stable during the calcination process and can support the desired mesostructure at high temperatures. The in situ nano-inorganic pore-makers can inhibit the excessive growth of crystals, thus improving the porosity of the mesostructure. Second, the in situ inorganic carbonate not only acts as the pore-maker but also as the reactant. Increasing the amount of one metal precursor leads to an increase in the dispersion of the other metal precursor in the dry gel. This enables the second metal precursor to completely react at low calcination temperatures, and this can result in a reduction in impurities caused by the second metal precursor. Although this strategy can tolerate phase separation to a certain extent, the surfactant P123 was used to protect

(1) Zukalova, M.; Zukal, A.; Kavan, L.; Nazeeruddin, M. K.; Liska, P.; Gratzel, M. *Nano Lett.* **2005**, *5*, 1789–1792.
(2) Baskaran, S.; Liu, J.; Domansky, K.; Kohler, N.; Li, X. H.; Coyle, C.; Fryxell, G. E.; Thevuthasan, S.; Williford, R. E. *Adv. Mater.* **2000**, *12*, 291–294.
(3) Yu, J. C.; Zhang, L. Z.; Zheng, Z.; Zhao, J. C. *Chem. Mater.* **2003**, *15*, 2280–2286.
(4) Yang, P. D.; Zhao, D. Y.; Margolese, D. I.; Chmelka, B. F.; Stucky, G. D. *Nature* **1998**, *396*, 152–155.
(5) Soler-illia, G. J. D.; Sanchez, C.; Lebeau, B.; Patarin, J. *Chem. Rev.* **2002**, *102*, 4093–4138.
(6) Grosso, D.; Cagnol, F.; Soler-Illia, G. J. D. A.; Crepaldi, E. L.; Amenitsch, H.; Brunet-Bruneau, A.; Bourgeois, A.; Sanchez, C. *Adv. Funct. Mater.* **2004**, *14*, 309–322.
(7) Grosso, D.; Boissiere, C.; Nicole, L.; Sanchez, C. *J. Sol-Gel Sci. Technol.* **2006**, *40*, 141–154.
(8) Narendar, Y.; Messing, G. L. *Catal. Today* **1997**, *35*, 247–268.
(9) Kakihana, M.; Yoshimura, M. *Bull. Chem. Soc. Jpn.* **1999**, *72*, 1427–1443.
(10) Cushing, B. L.; Kolesnichenko, V. L.; O'Connor, C. J. *Chem. Rev.* **2004**, *104*, 3893–3946.
(11) Grosso, D.; Boissiere, C.; Smarsly, B.; Brezesinski, T.; Pinna, N.; Albouy, P. A.; Amenitsch, H.; Antonietti, M.; Sanchez, C. *Nat. Mater.* **2004**, *3*, 787–792.
(12) Crepaldi, E. L.; Soler-Illia, G. J. D. A.; Bouchara, A.; Grosso, D.; Durand, D.; Sanchez, C. *Angew. Chem., Int. Ed.* **2003**, *42*, 347–351.
(13) Wei, X.; Xu, G.; Ren, Z. H.; Wang, Y. G.; Shen, G.; Han, G. R. *J. Am. Ceram. Soc.* **2008**, *91*, 299–302.
(14) Hou, B.; Li, Z. J.; Xu, Y.; Wu, D.; Sun, Y. H. *Nanoporous Mater. IV* **2005**, *156*, 465–472.
(15) Hou, R. Z.; Ferreira, P.; Vilarinho, P. M. *Microporous Mesoporous Mater.* **2008**, *110*, 392–396.

 Published on Web 01/08/2010

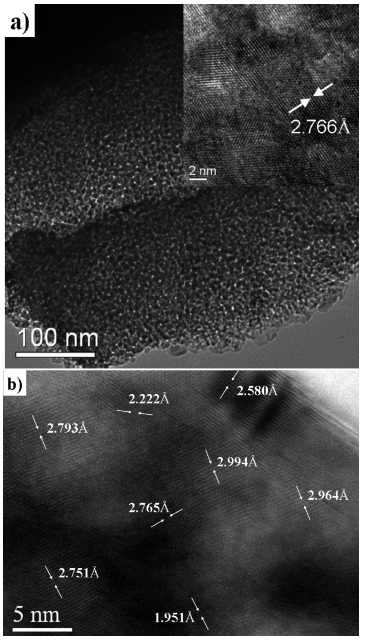

Figure 1. Transmission electron microscopy images of MST-1.5 after (a) and prior to (b) removing $SrCO_3$ pore-makers.

the dry gel from a bad phase separation and improve the specific surface area of the samples before the acid treatment. The obtained samples of mesoporous $SrTiO_3$ are abbreviated to MST-1, MST-1.5, and MST-2 according to their Sr/Ti ratios. For example, MST-1.5 means a mesoporous $SrTiO_3$ with a 1.5:1 Sr/Ti mol ratio.

Transmission electron microscopy (TEM) images of MST-1.5 in Figure 1a indicate that the sample has worm-like channels. The lattice plane spacing of the MST-1.5, estimated from the inset, is 2.766 Å, which could be indexed to (110) of $SrTiO_3$. Figure 1b shows a high-resolution TEM image of the MST-1.5, before removal of $SrCO_3$. The lattice planes of 2.793, 2.765, 2.751, and 1.951 Å correspond to (110), (110), (110), and (200) of $SrTiO_3$, while those of 2.580, 2.994, 2.964, and 2.222 Å are from (210), (200), (200), and (121) of $SrCO_3$, respectively. It can be seen that the $SrTiO_3$ nanocrystals are connected to each other and are mixed with the $SrCO_3$ nanocrystals. This phenomenon can be explained by the percolation theory.[16] In a two-phase system, when the volume fraction of the minor phase increases to a critical value, the grains can connect with each other to form a continuous random cluster (percolation-like cluster structure). Hence, the $SrCO_3$ and $SrTiO_3$ nanocrystals should both form percolation-like cluster structures.

X-ray diffraction (XRD) patterns (Figure 2) show that the MST-1, MST-1.5, and MST-2 samples belong to a $SrTiO_3$ phase (JCPDS No. 35-0734). The crystalline sizes of the MST-1, MST-1.5, and MST-2, calculated using the Scherrer equation, are 26.2, 12.9, and 10.3 nm, respectively. The reason why the crystalline size decreases with increasing Sr/Ti ratio is that the $SrCO_3$ acts as a diffusion barrier and inhibits the crystal growth of the

(16) Nan, C. W. *Prog. Mater. Sci.* **1993**, *37*, 1–116.

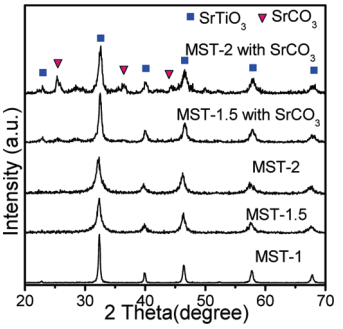

Figure 2. XRD patterns of MST-1, MST-1.5, MST-2, and MST-1.5 (MST-2) without removing $SrCO_3$ pore-makers.

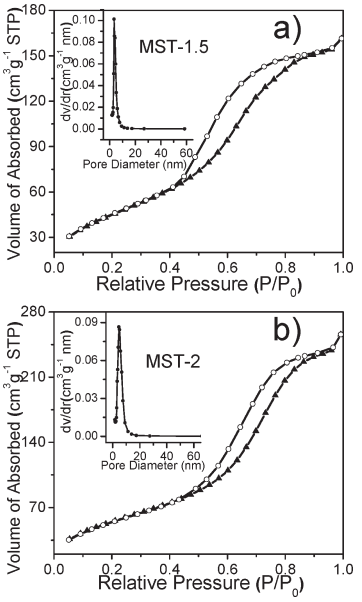

Figure 3. N_2 adsorption−desorption isotherm and pore size distribution (inset) of MST-1.5 (a) and MST-2 (b).

nanocrystalline $SrTiO_3$. From the XRD patterns of MST-1.5 and MST-2, prior to removal of $SrCO_3$, it can be seen that the excess Sr precursor exists in the form of $SrCO_3$ nanocrystals in the calcined samples.

The N_2 adsorption−desorption isotherms of MST-1.5 and MST-2 (Figure 3) reveal a stepwise adsorption and desorption process, which is characteristic of mesoporous materials. The specific surface areas are 46, 169, and 206 m^2/g for MST-1, MST-1.5, and MST-2, respectively. Increasing the number of Sr precursors leads to an increase in the specific surface area. This increase is mainly due to the increased number of $SrCO_3$ pore-makers, which means they can form more channels. MST-2 exhibits a larger Barrett−Joyner−Halenda (BJH) average pore diameter (5.4 nm) than MST-1.5 (4.3 nm). This phenomenon may be ascribed to the fact that more $SrCO_3$ nanocrystals tend to form larger sized grains corresponding to larger pore diameters. Combined with the XRD results, it can be seen that MST-2 with a smaller crystalline size has a larger pore size diameter. The reason for this is that a larger quantity of $SrCO_3$ will correspond to thicker diffuse barriers and therefore a stronger ability to inhibit $SrTiO_3$ crystal growth. The specific surface

Scheme 1. Mechanism of Formation of Mesoporous $SrTiO_3$[a]

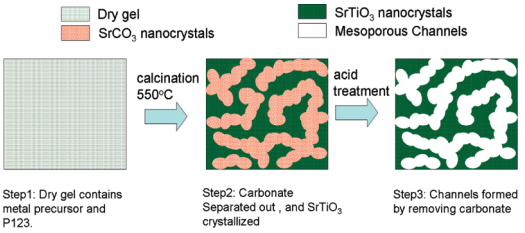

[a] Step 1: After solvent is evaporated, the dry gel with the metal precursor and P123 were formed. Step 2: After high temperature calcination, the in situ $SrCO_3$ pore-makers crystallized and $SrTiO_3$ formed. The nanocrystalline $SrTiO_3$ particles connected to each other and formed random mesoporous structures as well as percolation-like cluster structures. Step 3: The $SrCO_3$ pore makers were removed by an acidic solution, channels were released, and the mesostructure of $SrTiO_3$ was obtained.

areas of MST-1.5 and MST-2, before the acid treatment, are 28.2 and 19.2 m^2/g, respectively, which is attributed to the channels formed by the P123 surfactant. These channels benefit from the introduction of acid into the interior of the samples and help to completely dissolve the $SrCO_3$.

From the above analysis, a possible mechanism for the mesoporous $SrTiO_3$ formation is shown in Scheme 1. It is believed that excess carbonate plays a role as pore-maker, because the $SrCO_3$ nanocrystals can be removed completely by acid and the specific surface area increased. The key point of this successful strategy is that the excess carbonate acts as a diffusion barrier to inhibit the crystal growth of $SrTiO_3$. Small crystalline size is beneficial to the existence of thin pore walls and high porosity mesostructures. This strategy has also been successful in obtaining mesoporous crystalline $BaTiO_3$ (MBT-1.5) with a large specific surface area of 167 m^2/g, which is larger than that of any other mesoporous $BaTiO_3$ which has been reported (shown in Supporting Information).

UV−vis absorption spectra of the samples were investigated (Figure 4). The band gaps of ST, MST-1, MST-1.5, and MST-2 were estimated to be 3.17, 3.18, 3.24, and 3.25 eV, respectively. The absorption spectra show an obvious blue shift caused by the quantum size effect. Similarly, the MBT-1.5 with a smaller crystal size (13.2 nm) possesses a larger band gap (3.2 eV) than BT (3.11 eV, crystal size >100 nm) prepared by a solid state reaction.

Mesoporous multimetal oxides with large specific surface areas and crystalline pore walls have potential applications in photocatalysis. Therefore we also studied the photocatalytic properties of the obtained mesoporous $SrTiO_3$ and $BaTiO_3$. The photocatalytic activities of the samples were evaluated by oxidative dehydrogenation of 2-propanol to acetone under light irradiation ($\lambda >$ 300 nm). For comparison, using a traditional solid-state reaction, small specific surface area $SrTiO_3$ (ST) and $BaTiO_3$ (BT) were also synthesized. Figure 5 shows the conversion of the 2-propanol to acetone over the different samples. After 30 min of photocatalytic reaction, the conversion ratios of the 2-propanol to acetone for ST,

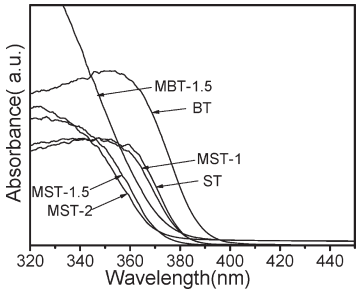

Figure 4. UV−vis absorbance spectra of samples, ST and BT, are $SrTiO_3$ and $BaTiO_3$ synthesized by solid-state reaction.

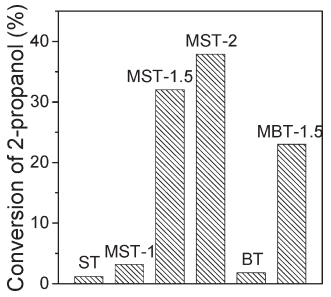

Figure 5. Photocatalytic conversion ratios of 2-propanol to acetone on the samples at the same photocatalytic reaction time.

MST-1, MST-1.5, MST-2, BT, and MBT-1.5 were 1.2%, 3.2%, 32%, 38%, 1.8%, and 23%, respectively. Blank experiments show the conversion is indeed photocatalytically induced (detailed in Supporting Information). The mesoporous $SrTiO_3$ and $BaTiO_3$ both exhibit much higher activities than those of the samples prepared by the solid-state reactions. The enhanced photocatalytic activities of the mesoporous samples can be attributed to the large specific surface areas that provide a larger number of active sites for the catalytic reaction.

In summary, a new strategy, using in situ carbonate as a pore-maker, has been adopted to synthesize crystalline mesoporous multimetal oxide $SrTiO_3$ and $BaTiO_3$. The obtained samples have large specific surface areas, narrow pore-size distributions, and higher photocatalytic activities. A prerequisite for the formation of mesoporous multimetal oxides is that the carbonate must not thermally degrade below and at the temperature of crystallization of the desired materials. Since the decomposition temperatures of most carbonates are usually higher than 700 °C,[17] the strategy could be applied to synthesize other mesoporous multimetal oxides.

Acknowledgment. Financial support from the National Basic Research Program of China (No. 2007CB613305) and the National Natural Science Foundation of China (Nos. 20603017, 50732004, 20773064, and 10874077) is gratefully acknowledged.

Supporting Information Available: Experimental section, TG-DSC, XRD, N_2 sorption, blank experiments, and data of obtained mesoporous $BaTiO_3$ (PDF). This material is available free of charge via the Internet at http://pubs.acs.org.

(17) L'vov, B. V. *Thermochim. Acta* **2002**, *386*, 1–16.